International Journal of Extreme Manufacturing

Laser-assisted growth of hierarchically architectured 2D MoS_2 crystals on metal substrate for potential energy applications

OPEN ACCESS
IOP Publishing | IMMT
International Journal of Extreme Manufacturing
Int. J. Extrem. Manuf. 4 (2022) 045102 (10pp)
https://doi.org/10.1088/2631-7990/ac8f73

Laser-assisted growth of hierarchically architectured 2D MoS_2 crystals on metal substrate for potential energy applications

Parvin Fathi-Hafshejani[1], Jafar Orangi[2], Majid Beidaghi[2] and Masoud Mahjouri-Samani[1,*]

[1] Department of Electrical and Computer Engineering, Auburn University, Auburn, AL 36849, United States of America
[2] Department of Mechanical and Material Engineering, Auburn University, Auburn, AL 36849, United States of America

E-mail: mahjouri@auburn.edu

Received 20 January 2022, revised 3 June 2022
Accepted for publication 5 September 2022
Published 20 September 2022

Abstract

Recently, there has been substantial interest in the large-scale synthesis of hierarchically architectured transition metal dichalcogenides and designing electrodes for energy conversion and storage applications such as electrocatalysis, rechargeable batteries, and supercapacitors. Here we report a novel hybrid laser-assisted micro/nanopatterning and sulfurization method for rapid manufacturing of hierarchically architectured molybdenum disulfide (MoS_2) layers directly on molybdenum sheets. This laser surface structuring not only provides the ability to design specific micro/nanostructured patterns but also significantly enhances the crystal growth kinetics. Micro and nanoscale characterization methods are employed to study the morphological, structural, and atomistic characteristics of the formed crystals at various laser processing and crystal growth conditions. To compare the performance characteristics of the laser-structured and unstructured samples, Li-ion battery cells are fabricated and their energy storage capacity is measured. The hierarchically architectured MoS_2 crystals show higher performance with specific capacities of about 10 mAh cm^{-2}, at a current rate of 0.1 mA cm^{-2}. This rapid laser patterning and growth of 2D materials directly on conductive sheets may enable the future large-scale and roll-to-roll manufacturing of energy and sensing devices.

Supplementary material for this article is available online

Keywords: 2D materials, laser manufacturing, laser patterning, energy applications, Li-ion battery

* Author to whom any correspondence should be addressed.

2631-7990/22/045102+10$33.00

1. Introduction

Transition metal dichalcogenides (TMDCs) have recently emerged as a significant class of layered materials with a number of applications in electronics, photonics, energy storage, catalysis, and sensing devices [1–11]. The chemical composition of TMDCs has been expressed by MX_2 (M = transition metal, and X = chalcogen), where the transition metal is sandwiched in between chalcogen atoms forming a three-atom thick two-dimensional (2D) crystalline layer. The bulk structure of the TMDCs consists of repeating layers with weak van der Waals bonding between the layers and strong covalent interaction within the layers [12–15].

Among various areas of application, energy applications such as catalysis, energy generation, and storage have been promising areas of interest for 2D TMDC materials [16–21]. For instance, in lithium cells, transition metal sulfides (TMSs) have been important cathode materials [16, 22–24] where the lithium is stored in their lattices by the intercalation/deintercalation processes. Molybdenum disulfide (MoS_2) is one of the promising electrode materials, among the TMSs, for rechargeable lithium-ion batteries [23, 25–28]. The layered structure of MoS_2 allows foreign molecules or ions to easily move between the layers through the intercalation/deintercalation processes [29–34].

Mono and few-layer TMDC nanosheets can be synthesized by bottom-up atom-by-atom growth processes or top-down mechanical and chemical exfoliation of bulk 2D materials [22, 35–38]. In the bottom-up atom-by-atom method, TMDCs are typically grown on different substrates (e.g. S/SiO_2) using physical or chemical vapor deposition methods [39, 40]. In the top-down method, stacked layers are separated into few-layer sheets using chemical and micromechanical cleavage methods [41]. The bottom-up atom-by-atom approach is a low yield, high cost, and time-consuming process, which is typically used for electronic and optoelectronic applications. For instance, there are some reports on industrial atomic layer deposition (ALD) and chemical vapour deposition (CVD) approaches for the wafer-scale depositions of TMDC's [42, 43]. The top-down mechanical and chemical exfoliation approach produces large-scale, low-cost, and fast 2D materials that are suitable for energy applications. However, mechanical and chemical exfoliation requires post-processing, slurry formation, patterning, and deposition onto conductive electrodes with reliable contact between 2D materials and metal substrates [44–47]. Therefore, large-scale, high yield, and low-cost direct syntheses approach with control over their structures, patterns, and interfaces are highly desired to manufacture 2D-based electrodes for energy applications.

Lasers applications in the synthesis and processing of 2D and other related energy materials has been an attractive area for large-scale, roll-to-roll, and low-cost manufacturing of energy devices [48–55]. Recently, laser processing has been become an attractive tool for enhancing manufacturing and improving battery performance. For instance, laser modification or ablation of electrode materials is now used to create various patterns and structures on the electrodes of the batteries [56–60]. This has directly influenced the electrochemical properties and greatly enhanced battery performance, including battery lifetime, high-rate capability, and cycle stability. One of the critical issues for thick film and high energy electrodes is improving the electrode film adhesion, which can be possible by laser structuring [61–63]. Hence, a new battery concept has been introduced by the direct laser structuring of electrodes for achieving large-area energy capacities and power densities [64–67].

The wide choice of lasers with various power, energy, and timescales (from continuous-wave to femtoseconds) has enabled their use in many industrial-scale manufacturing sectors for rapid (e.g. a few thousand mm s^{-1}), high precision, and low-cost processing needs. Accordingly, this work presents the use of laser processing for rapid laser patterning and large-scale manufacturing of 2D materials with high-quality and high growth rate directly on conductive transition metals sheets. This method has the potential to be adopted in the future roll-to-roll industrial level energy device manufacturing. Besides improving the quality and growth rate, this method offers large-scale rapid manufacturing of 2D materials directly on the conductive transition metal substrates for future roll-to-roll industrial level energy device manufacturing. Here, we report a unique solution for the formation of designed patterns and hierarchically architectured high-quality 2D MoS_2 crystals directly on molybdenum substrates to design electrodes for 3D batteries. This process combines the flexibility and advantages of the laser structuring method to create micro/nanostructures on molybdenum substrates, followed by sulfurization and the growth of high-quality MoS_2 crystals in the patterned structures. The laser micro/nanopatterning provides the ability to design desired architectures and channels on the substrates and highly enhances the sulfur diffusion and crystal growth kinetics resulting in high yield growth of 2D crystals. Moreover, since the 2D crystals grow directly from and penetrate into the conductive substrate (Mo), there is a natural chemical bond between the 2D material and the substrate that eliminates the use of a binder for adhesion. Thus this method could be more resilient to bending. We show that the crystals are, in fact, pure with the desired quality and with suitable battery performance characteristics.

2. Results and discussion

2.1. Growth of hierarchically architectured 2D MoS_2 crystals

As shown in figure 1, to create designed patterns with controlled architectures and dimensions, molybdenum substrates (99.9% purity) were precisely laser structured (see Supplementary data) in an argon environment to avoid unwanted chemical reactions and oxidation. The laser-structured substrates were then controllably sulfurized inside a tube furnace under atmospheric argon pressure and at various temperatures. After loading the samples and sulfur boat into the tube furnace, first, the tube was vacuumed down to ~1 mtorr, followed by argon purging for a few minutes. Then the tube was filled with 500 mtorr of argon, and the sulfurization processes were studied under various temperatures (e.g. 400 °C–900 °C) and time. The sulfurization was achieved by evaporating 10 mg

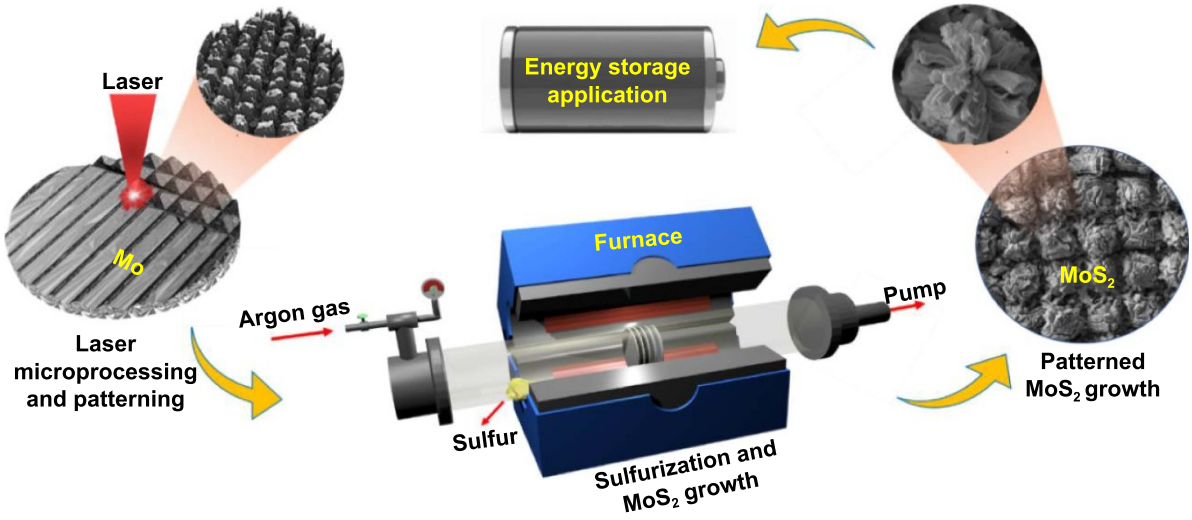

Figure 1. Schematic a hybrid method for non-coating fabrication of substrate grown MoS_2 growing directly from Mo substrate with laser assistant.

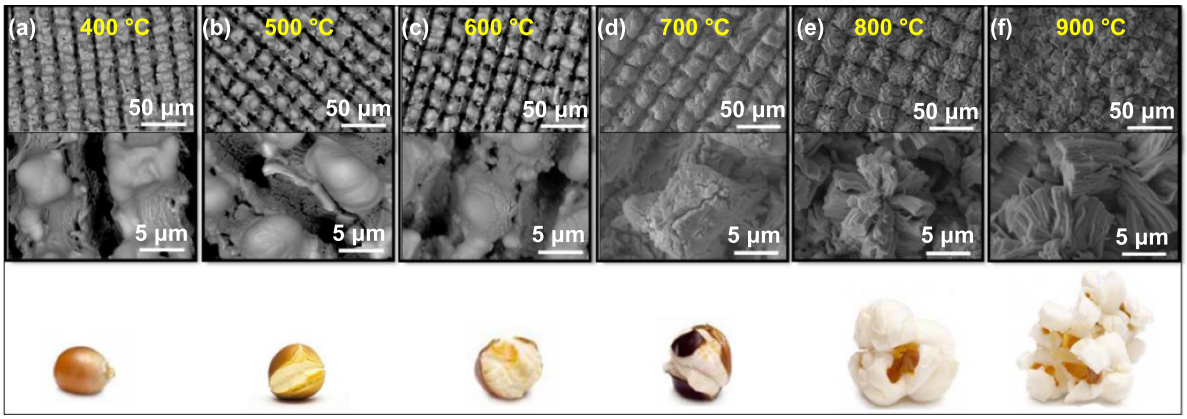

Figure 2. Low and high magnification SEM images showing the morphology of synthesized MoS_2 in different sulfurization temperatures. The MoS_2 sulfurized at 400 °C (a), 500 °C (b), 600 °C (c), 700 °C (d), 800 °C (e), and 900 °C (f). The popcorn analogy is used to demonstrate the temperature-dependent evolution of the MoS_2 growth in the process.

of sulfur powder in the low-temperature zone of the furnace. The furnace temperature helps dissociate the vaporized sulfur molecules to smaller chemically activate S species. The large sulfur molecules such as S_6, S_7, and S_8 are the dominant species in the vapor at low temperatures of about 150 °C. However, at relatively temperatures above 500 °C, the smaller molecules such as S_4, S_3, and S_2 become dominant [68, 69]. Therefore, the sulfur vapor close to the samples zone are expected to be a highly reactive smaller species that can diffuse into the molybdenum substrate and form MoS_2 structures.

In order to verify the temperature effect on the formation of MoS_2 crystals, different sulfurization temperatures ranging from 400 °C to 1000 °C were tested. The surface morphologies and physical structures of the synthesized MoS_2 samples were studied using a profilometer (see Supplementary data) and scanning electron microscopy (SEM). As shown in figure 2, the SEM images of the samples revealed a popcorn-like growth evolution of the MoS_2 crystals as a function of substrate temperatures. When the temperature increases, sulfur species highly react with Mo and diffuse far inside the microstructures. Since the density of Mo is almost twice the density of MoS_2, the MoS_2 will need twice the space of Mo. Thus, it begins to crack the microstructure and expand outward.

For instance, the initial sign of MoS_2 growth was observed at 400 °C. As the temperature was increased for a constant reaction time of 10 min, molybdenum structures started cracking, and larger MoS_2 flakes started springing out. At 700 and 800 °C large flower-like MoS_2 crystals were formed, covering the entire structure. The higher sample temperatures (i.e. 900 °C and 1000 °C) provided both higher thermal energy for diffusion during the sulfurization process and increased the reactive S species resulting in the enhanced growth of the crystals. The growth was so high that the microstructures and microchannels on the substrates disappeared. However, signs

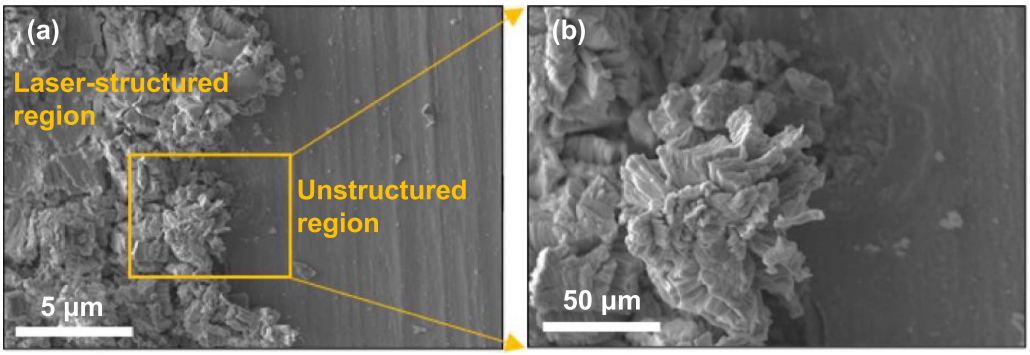

Figure 3. Low (a) and high (b) magnification SEM images of MoS_2 synthesized at 800 °C on a substrate with half laser-structured and the other half unstructured. Laser surface structuring not only provides flexibility in designing the desired structures but also enhances the sulfurization and growth processes.

of decompositions and degradation of MoS_2 crystals were observed in TEM images (see Supplementary data) when the temperature was increased to 900 °C and beyond.

The micro/nanostructures formed by the laser processing significantly increase the surface area for sulfur interaction and diffusion, leading to more sulfurization and MoS_2 growth than in unstructured regions. To show how laser structuring makes a huge difference in the sulfurization and enhanced growth of MoS_2 crystals and confirm our hypotheses, we compared the growth of MoS_2 crystals on both laser-structured and unstructured molybdenum substrates side by side. To perform this experiment, half of a molybdenum substrate was laser patterned, and the other half was kept intact. The sample was then loaded into the tube furnace, and MoS_2 growth was performed at 800 °C. As shown in figure 3, the laser-structured regions showed a much higher growth rate than the unstructured region. The unstructured region only formed a few-layer coating on the surface, while the laser-structured region experienced enhanced growth with flower-like structures.

To assess the quality and structure of the synthesized MoS_2 crystals at different temperatures, samples were carefully characterized by Raman spectroscopy and x-ray diffraction (XRD), as shown in figure 4. The Raman spectra of the MoS_2 crystals (figure 3(a)) prepared at different temperatures clearly showed the in-plane (E^1_{2g}) mode at 383 cm^{-1} and an out-of-plane (A_{1g}) mode at 407 cm^{-1}. The interval between the E^1_{2g} and A_{1g} peaks was about 24 cm^{-1}, similar to the reported value for the bulk MoS_2 crystals. By increasing the growth temperature, the difference between E^1_{2g} and A_{1g} peaks gets larger, indicating the formation of thicker layered structures at higher temperatures [12, 70]. The asymmetric and broad peaks at 454 cm^{-1} is due to the superposition of the first-order optical phonon A2u and second-order 2LA(M) vibrational modes [71, 72]. The intensity of the peaks increased for higher temperature samples, possibly due to the higher density of MoS_2 crystals grown at higher temperatures, as also confirmed by the SEM. At lower temperatures, since the MoS_2 growth is much less and slightly covers the samples' surface, the Raman intensity was not as strong as the high-temperatures grown samples.

As shown in figure 4(b), the MoS_2 crystals at higher temperatures (>600 °C) show a strong diffraction peak at $2\theta = 14.4°$ corresponding to the (002) face, indicating the multilayer nature of the structures. As the temperature increases, this peak becomes stronger, which means the number of layers has increased. Besides, other smaller peaks located at $2\theta = 32°$, 39.5°, 58°, and 60.2° can be observed, which are assigned to the (002), (100), (103), (110), and (008) face, respectively (Joint Committee on Powder Diffraction Standards (JCPDS) 37-1492). If the material is monolayer or too thin, XRD typically does not show any peaks since constructive interference cannot be formed. Also, as the temperature goes up, molybdenum peaks (at $2\theta = 40.6°$, 58.5°, 73.7°) disappear due to increased MoS_2 thickness. Figures 4(c) and (d) compare the Raman and XRD spectra of the sample grown at 800 °C with and without laser structuring. The corresponding MoS_2 Raman peaks at 383 and 407 cm^{-1} (figure 4(c)) and diffraction peak at $2\theta = 14.4°$ (figure 4(d)) show much stronger intensity than the unstructured samples due to the higher growth of the structured regions compared to the unstructured.

To gain atomistic information regarding the quality and structure of the synthesized MoS_2 crystals, scanning transmission electron microscopy (STEM) images we obtained and analyzed. Figure 5 shows the STEM images of stacked MoS_2 crystals synthesized at 800 °C that clearly shows the layered nature of the material formed by a number of monolayers attached together via van der Waals forces. The hexagonal atomic arrangement of the Mo and S atoms is observed, confirming the 2H crystalline phases of the crystals, as shown in figure 5(b). The fast Fourier transform (FFT) pattern (inset in figure 5(b)) taken from this monolayer crystal shows a hexagonal pattern corresponding to MoS_2 crystals as expected. Moreover, figure 5(c) shows the close-up view of the atomic arrangements with well-defined hexagonal symmetry. The brighter spots are Mo atoms, and the dimer spots are two sulfur atoms lined up on top of each other. This is further confirmed by the intensity profile of the crystals, as shown in figure 5(d). It should be noted that, according to the STEM images, samples grown at a higher temperature (e.g. 900 °C) showed a minor sign of decomposition at the edges of the flakes (see Supplementary data).

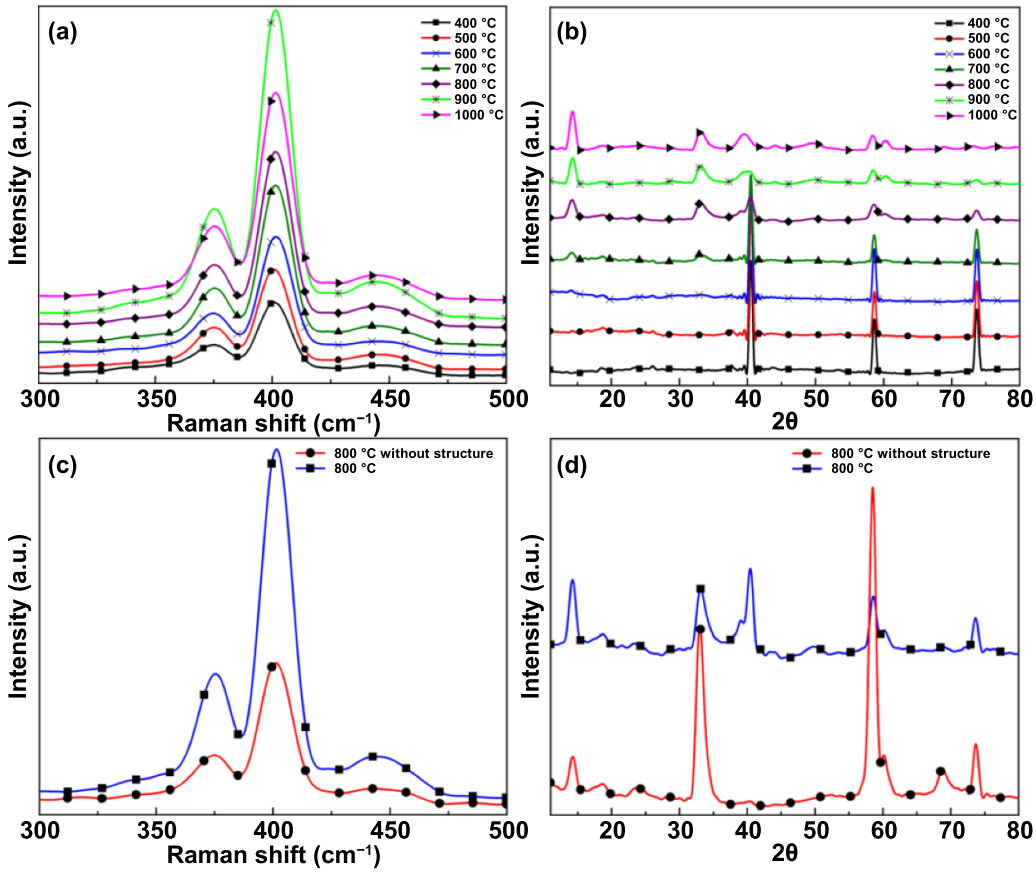

Figure 4. Raman (a) and XRD (b) spectra of the grown MoS_2 structures on Mo samples demonstrating the evolution of the MoS_2 crystals at various growth temperatures. Comparison of the Raman (c) and XRD (d) spectra of the MoS_2 samples grown at 800 °C on laser-structured (blue) and unstructured (red) molybdenum surfaces.

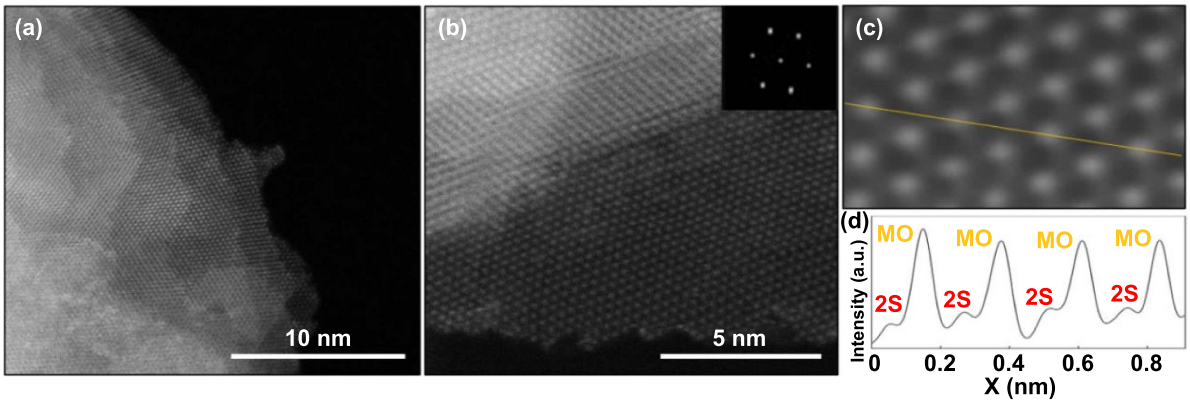

Figure 5. STEM characterization of the synthesized MoS_2 crystals. High magnification STEM images (a), (b) and FFT of the crystal (inset in (b)) showing highly crystalline layered materials with hexagonal crystal structures as expected for MoS_2. Close-up view (c) and the intensity line profile (d) showing Mo and 2S atoms in the crystals.

2.2. Electrochemical performance in a rechargeable Li-ion battery

The preliminary studies of electrochemical properties of structured MoS_2 crystals were performed using electrodes fabricated on 10 mm diameter Mo substrates. The weight of the synthesized MoS_2 crystals on the cells was measured by weighing the samples after the laser structuring and sulfurization processes (three times for each sample) with 1 μg measurement accuracy. The differences in the measured weights were basically the amount of sulfur added to the substrate during the formation of MoS_2 crystals. Since there are two sulfur atoms for each Mo atom in a unit formula of MoS_2, and considering the atomic mass of Mo and S, it was possible to estimate

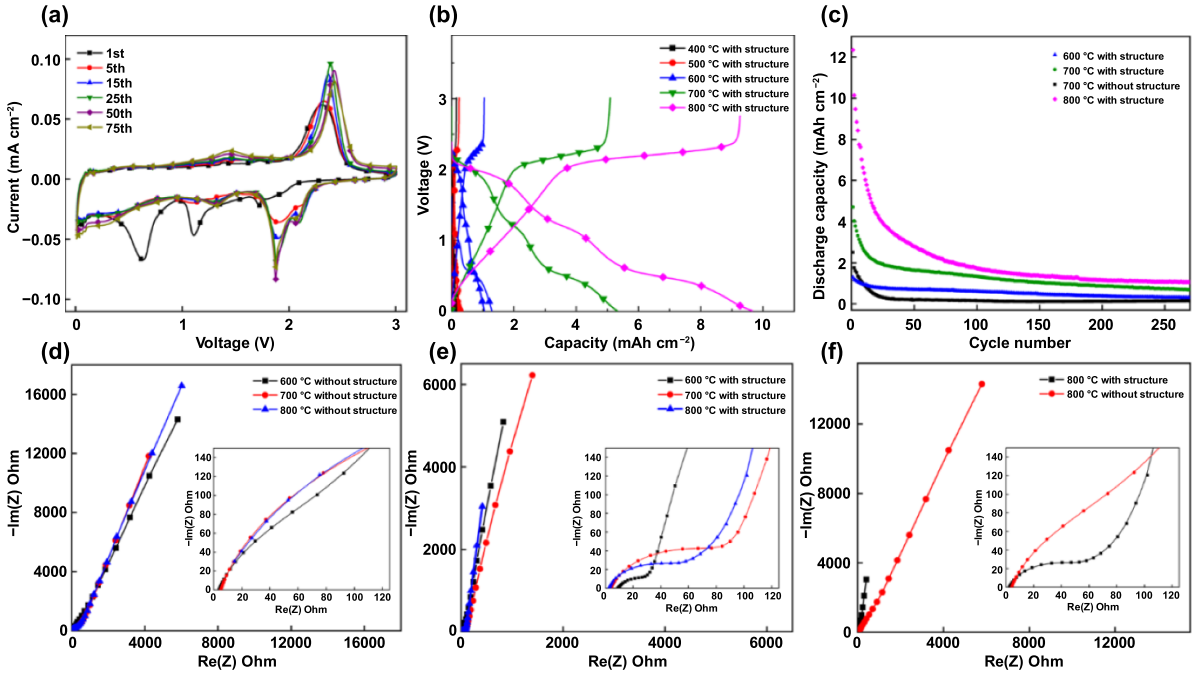

Figure 6. Electrochemical measurements of the fabricated MoS_2 electrodes. (a) CV curves for the first 75 cycles at a scan rate of 0.2 mV s^{-1}. (b) GCD curves of the MoS_2 electrode fabricated at different heat treatment temperatures. (c) Discharge capacities of electrodes with laser structuring heat-treated at 600 °C, 700 °C, and 800 °C, and unstructured electrodes heat-treated at 700 °C. EIS of MoS_2 electrodes at different sulfurization temperatures (d) without and (e) with laser structuring. (f) EIS of laser-structured and unstructured electrodes at 800 °C.

the total MoS_2 weight in the fabricated electrodes. The MoS_2 weight clearly increases as a function of growth temperature, consistent with other experimental observations mentioned above (figure S4).

The electrochemical properties of hierarchically architectured MoS_2 crystals and the potential of fabricated films as electrodes for Li-ion batteries or Li-ion capacitors were investigated by studying the behavior of the electrodes during the electrochemical intercalation of Li ions. We hypothesized that the processing conditions would impact the electrochemical properties of the MoS_2 films by affecting the electrodes' surface area and the diffusion path of Li ions. As shown in figure 6(a), the first discharge cycle of the cyclic voltammetry (CV) test showed two peaks, similar to the corresponding galvanostatic charge/discharge (GCD) curves (figure 6(b)). As previously reported, the peak observed at 1.1 V is due to the Li-ion insertion reaction forming Li_XMoS_2, and the peak at 0.6 V is related to the MoS_2 conversion reaction (transformation from trigonal prisms to an octahedral phase) [27, 73, 74]. These peaks on the discharge curve disappear in the following cycles, and a peak corresponding to the insertion of Li ions into the layered MoS_2 appears at about 1.9–2.1 V. The peak at 2.3–2.4 V in the charge curve corresponds to the Li extraction from the structure of layered MoS_2 [74]. Figure 6(b) shows the (GCD behavior of the fabricated cells with laser-structured MoS_2 electrodes fabricated at different temperatures. Similar voltage profiles of different samples for the first discharge cycle at the low current density of 50 mA cm^{-2} indicate similar electrochemical characteristics, with two discharge plateaus at around 1.1–1.4 V and 0.6 V, in agreement with previous reports [75–77]. In addition, the voltage profiles of laser-structured samples at 700 °C, at different current densities are shown in figure S5.

Samples fabricated at different temperatures were galvanostatically cycled at different current densities. The results of cycling tests of various electrodes are presented in figure 6(c). Comparing the specific capacity of laser-structured *vs.* unstructured electrodes fabricated at 700 °C shows a significant improvement in capacity, approximately 50%, for the laser-structured electrode. Also, the cycling performance significantly improved (figure 6(c)), which can be attributed to the open channels between the MoS_2 layers and more space available for expansion/contraction of MoS_2 crystals during the insertion/extraction of Li ions. Similar behavior was observed for the electrodes fabricated at different temperatures with and without laser structuring (figure S6). In addition, the results presented in figure 6(c) show that increasing the heat treatment process significantly increases the specific capacity of the electrodes, mainly due to the higher amount of MoS_2 crystals formed at higher temperatures.

The enhanced electrochemical performance of laser-structured electrodes can potentially be originated from two mechanisms. First, it can be related to the Li ion transfer paths created by laser structuring, which facilitate the transport of ions in and out of the electrodes. Indeed, the flake-like form of the 2D MoS_2 crystals can slow down ion transport into the bulk of the electrode, and laser structuring can significantly

shorten the ion diffusion path by providing electrolyte access to the MoS_2 flakes and enhancing the intercalation of Li ions between the flakes. Another possible reason is the improved sulfurization of Mo after laser structuring, as discussed above. The improved sulfurization increases the amount of the active material on the Mo substrates leading to their higher specific capacity [57, 59, 78].

Further insight into the electrochemical properties of the electrodes was achieved through electrochemical impedance spectroscopy (EIS). The data were obtained in 100 mHz to 1000 kHz frequency range at the open circuit potential and using a voltage amplitude of 10 mV. Figures 6(d) and (e) present the Nyquist plots of electrodes at various sulfurization temperatures without and with laser structuring. The almost vertical rise of the imaginary impedance (-Im(Z)) and the lower impedance values at low frequencies, in agreement with the results of other electrochemical tests, show the higher capacity and ion transport properties of the laser-structured electrodes. However, the Nyquist plots also show the appearance of semi-circle features at higher frequencies for laser-structures electrodes that do not exist for the electrodes without structuring. This semi-circle feature is associated with charge transfer resistance of the electrodes. This is because laser-structuring improves the ion accessibility of MoS_2 flakes, and the charge storage is based on the intercalation of the Li ions between MoS_2 flakes. However, for the electrode without structuring, it appears that the charge storage is limited to the surface of MoS_2, and these electrodes show a more capacitive charge mechanism. This difference between the EIS behavior of the electrodes is highlighted in figure 6(f), where the Nyquist plots of the electrodes heat treated at the same temperature of 800 °C are compared. It is worth noting that figures 6(d) and (e) show that laser structuring has a more significant impact on the electrochemical performance of the electrodes compared to the heat treatment temperature.

3. Conclusion

In conclusion, we demonstrated a unique hybrid laser-assisted structuring and sulfurization method for the formation of hierarchically architectured high-quality 2D MoS_2 crystal directly on molybdenum substrates. This work verified that laser structuring significantly enhances the sulfurization and MoS_2 growth rate and enables morphological control over the synthesis of MoS_2 crystals. We also showed the effect of sulfurization temperatures on the formation and the quality of the MoS_2 crystals. The SEM images of the MoS_2 crystals showed a popcorn-like growth evolution as a function of sulfurization temperature. The energy storage capability of the samples was tested by preparing Li-ion cells and measuring their performance. The MoS_2 nanosheets show the specific capacities of 10 mAh cm^{-2}, at a current rate of 0.1 mA cm^{-2}, proving the effectiveness of laser structuring in enhancing the Li storage properties of fabricated MoS_2 electrodes. This rapid laser patterning and large-scale manufacturing of 2D materials directly on conductive sheets enable their application in future roll-to-roll industrial level energy and sensing device manufacturing.

4. Experimental

4.1. Laser structuring of the molybdenum surface

First, 0.5 mm thick Mo foil (0.25 mm thick, annealed, 99.95%) was cut into small disks of 10 mm in diameter and ultrasonically cleaned in acetone and methanol for 10 min. Then, the Mo disks were precisely structured by a 130 W tunable nanosecond fiber laser (SPI RedEnergy, wavelength = 1064 nm, pulse-width = 5 ns–2000 ns, repetition rate = 1 Hz–4 MHz) under argon atmosphere pressure to prevent unwanted chemical reactions and oxidation. A scanning galvanometer with an F-theta lens (∼12 μm spot size) and a designated software was used to control the laser scanning patterns. In the laser processing step, the goal was to create a deep and neat structure for proof of concept. Thus, various parameters such as power, speed, and pulse duration were tested to reach the desired ablation rates and structures. A scan speed of 1000 mm s^{-1}, laser power of 60–80 W, hatch distance 25 μm, and laser pulse-width of 508 ns produced the desired structured surfaces for this study. Our laser spot size diameter determined the laser processing resolution at the focal point (∼12 μm). Smaller spot sizes can push the feature sizes to lower limits. To create square patterns, vertical and horizontal lines were laser scanned on the surface with desired sizes and periodicities. For deeper structures, the laser scanning process was repeated a few times on the same pattern. After the laser structuring, samples were ultrasonically cleaned in acetone and methanol for 10 min to remove the loose laser-generated coating from the surface. It should be noted that shorter pulse-width lasers such as femtosecond and picosecond lasers could be more efficient for surface structuring and future upscaling and are worth the investigation.

4.2. Sulfurization and MoS_2 crystal growth

Prepared Mo samples were placed inside a 1-inch tube furnace. First, the system was pumped down to a few millitorrs and argon gas was used to purge the tube and remove the residual molecules. Then the pressure was raised to about 500 torr by backfilling argon gas into the tube. The temperature was set to the desired growth temperatures (400 °C–1000 °C). Solid sulfur granules (99.9995%) were located at the beginning of the quartz tube with the temperature of about 150 °C to slowly evaporate the sulfur. The evaporated sulfur then reaches the Mo substrates near the center of the tube furnace and reacts with Mo to grow MoS_2 crystals for the desired time. Finally, the system was turned off and naturally cooled down to room temperature.

4.3. Characterization

4.3.1. Raman spectroscopy. A home-built confocal Raman machine with a Horiba HR spectrometer and 1200 grooves mm^{-1} grating was used for optical spectroscopy.

A 50× microscope objective lens (numerical apperture (NA) = 0.75) and a 532 nm laser were used for data acquisition.

4.3.2. XRD measurements. Powder XRD (D8 Discover XRD system) was used to further verify the formation of crystalline MoS_2 in these experiments. Scans were conducted between 2θ angles ranging from 0° to 90°.

4.3.3. STEM characterization. An aberration-corrected Hitachi HD2700 STEM working at 80 kV or 120 kV was used for imaging. The detectors inner angles were set to 70 mrad, 40 mrad and 25 mrad, corresponding to high, medium, and low angle annular dark field imaging.

4.3.4. Measurement, analysis, and Li ion storage properties. To analyze the electrochemical properties of samples, a standard coin cells (CR-2032, MTI, Richmond, CA, USA) were used. The disk-shaped MoS_2 samples were placed on copper current collectors and tested as working electrodes. Lithium metal foil was used for the counter and reference electrodes and a polypropylene membrane (Celgard, Inc., Charlotte, NC) was used as the separator. 1M lithium hexafluorophosphate solution in ethylene carbonate and diethylcarbonate (1.0M LiPF6 in EC/DEC:50/50 (v/v)) was used as the electrolyte. To conduct the CV, a potentiostat (Biologic VMP3) with a scan rates of 0.2 mV s^{-1} was used in these experiments. A battery tester (LANDT, China) was used to test the coin cells in a galvanostatic mode with a range of 0.01–3.01 V with respect to Li.

Acknowledgments

This research was partially funded by the U.S. National Science Foundation (NSF) under Grant No. 1923363. We thank the Materials Characterization Facility at the Institute for Electronics and Nanotechnology (IEN) for aberration-corrected STEM Hitachi HD2700 measurements. Thanks to Alabama Micro/Nanoelectronic Science and Technology Center (AMNSTC) for providing access to the cleanroom facility. Also, thanks to S Elafandi for helping with the SEM imaging.

Author contributions

P F designed and executed the laser processing/structuring and synthesis experiments, sample characterizations, and analysis. J O and M B performed the electrochemical tests and analysis and participated in discussions and manuscript preparation. M M S led the project, led the design of experimental, participated in the data analysis, discussions, and manuscript preparation. The authors all read and commented on the manuscript.

Conflict of interest

The authors declare no conflict of interest.

ORCID iD

Masoud Mahjouri-Samani https://orcid.org/0000-0002-6080-7450

References

[1] Chhowalla M, Shin H S, Eda G, Li L J, Loh K P and Zhang H 2013 The chemistry of two-dimensional layered transition metal dichalcogenide nanosheets *Nat. Chem.* **5** 263–75
[2] Geim A K and Grigorieva I V 2013 Van der Waals heterostructures *Nature* **499** 419–25
[3] Wang Q H, Kalantar-Zadeh K, Kis A, Coleman J N and Strano M S 2012 Electronics and optoelectronics of two-dimensional transition metal dichalcogenides *Nat. Nanotechnol.* **7** 699–712
[4] Lee G H *et al* 2013 Flexible and transparent MoS_2 field-effect transistors on hexagonal boron nitride-graphene heterostructures *ACS Nano* **7** 7931–6
[5] Jariwala D, Sangwan V K, Lauhon L J, Marks T J and Hersam M C 2014 Emerging device applications for semiconducting two-dimensional transition metal dichalcogenides *ACS Nano* **8** 1102–20
[6] Mak K F, Lee C, Hone J, Shan J and Heinz T F 2010 Atomically thin MoS_2: a new direct-gap semiconductor *Phys. Rev. Lett.* **105** 136805
[7] Splendiani A, Sun L, Zhang Y B, Li T S, Kim J, Chim C Y, Galli G and Wang F 2010 Emerging photoluminescence in monolayer MoS_2 *Nano Lett.* **10** 1271–5
[8] Radisavljevic B, Radenovic A, Brivio J, Giacometti V and Kis A 2011 Single-layer MoS_2 transistors *Nat. Nanotechnol.* **6** 147–50
[9] Fang X P, Hua C X, Guo X W, Hu Y S, Wang Z X, Gao X P, Wu F, Wang J Z and Chen L Q 2012 Lithium storage in commercial MoS_2 in different potential ranges *Electrochim. Acta* **81** 155–60
[10] Bertolazzi S, Brivio J and Kis A 2011 Stretching and breaking of ultrathin MoS_2 *ACS Nano* **5** 9703–9
[11] Fathi-Hafshejani P, Azam N, Wang L, Kuroda M A, Hamilton M C, Hasim S and Mahjouri-Samani M 2021 Two-dimensional-material-based field-effect transistor biosensor for detecting COVID-19 virus (SARS-CoV-2) *ACS Nano* **15** 11461–9
[12] Lee C, Yan H G, Brus L E, Heinz T F, Hone J and Ryu S 2010 Anomalous lattice vibrations of single- and few-layer MoS_2 *ACS Nano* **4** 2695–700
[13] Gong Y J *et al* 2014 Vertical and in-plane heterostructures from WS_2/MoS_2 monolayers *Nat. Mater.* **13** 1135–42
[14] Ramakrishna Matte H S S, Gomathi A, Manna A K, Late D J, Datta R, Pati S K and Rao C N R 2010 MoS_2 and WS_2 analogues of graphene *Angew. Chem., Int. Ed.* **49** 4059–62
[15] Yin Z Y, Li H, Li H, Jiang L, Shi Y M, Sun Y H, Lu G, Zhang Q, Chen X D and Zhang H 2012 Single-layer MoS_2 phototransistors *ACS Nano* **6** 74–80
[16] Feng C Q, Ma J, Li H, Zeng R, Guo Z P and Liu H K 2009 Synthesis of molybdenum disulfide (MoS_2) for lithium ion battery applications *Mater. Res. Bull.* **44** 1811–5
[17] Carroll G M, Zhang H Y, Dunklin J R, Miller E M, Neale N R and van de Lagemaat J 2019 Unique interfacial thermodynamics of few-layer 2D MoS_2 for (photo) electrochemical catalysis *Energy Environ. Sci.* **12** 1648–56
[18] Naik S G and Rabinal M H K 2020 Molybdenum disulphide heterointerfaces as potential materials for solar cells, energy storage, and hydrogen evolution *Energy Technol.* **8** 1901299
[19] Li H Y, Jia X F, Zhang Q and Wang X 2018 Metallic transition-metal dichalcogenide nanocatalysts for energy conversion *Chem* **4** 1510–37

[20] Bissett M A, Worrall S D, Kinloch I A and Dryfe R A W 2016 Comparison of two-dimensional transition metal dichalcogenides for electrochemical supercapacitors *Electrochim. Acta* **201** 30–37
[21] Wang H, Feng H B and Li J H 2014 Graphene and graphene-like layered transition metal dichalcogenides in energy conversion and storage *Small* **10** 2165–81
[22] Truong Q D, Kempaiah Devaraju M, Nakayasu Y, Tamura N, Sasaki Y, Tomai T and Honma I 2017 Exfoliated MoS_2 and $MoSe_2$ nanosheets by a supercritical fluid process for a hybrid Mg–Li-ion battery *ACS Omega* **2** 2360–7
[23] Stephenson T, Li Z, Olsen B and Mitlin D 2014 Lithium ion battery applications of molybdenum disulfide (MoS_2) nanocomposites *Energy Environ. Sci.* **7** 209–31
[24] Wang G X, Bewlay S, Yao J, Liu H K and Dou S X 2004 Tungsten disulfide nanotubes for lithium storage *Electrochem. Solid-State Lett.* **7** A321–3
[25] Das S K, Mallavajula R, Jayaprakash N and Archer L A 2012 Self-assembled MoS_2–carbon nanostructures: influence of nanostructuring and carbon on lithium battery performance *J. Mater. Chem.* **22** 12988–92
[26] Chang K, Chen W X, Ma L, Li H, Li H, Huang F H, Xu Z D, Zhang Q B and Lee J Y 2011 Graphene-like MoS_2/amorphous carbon composites with high capacity and excellent stability as anode materials for lithium ion batteries *J. Mater. Chem.* **21** 6251–7
[27] Chang K and Chen W X 2011 L-cysteine-assisted synthesis of layered MoS_2/graphene composites with excellent electrochemical performances for lithium ion batteries *ACS Nano* **5** 4720–8
[28] Zhang C F, Wu H B, Guo Z P and Lou X W 2012 Facile synthesis of carbon-coated MoS_2 nanorods with enhanced lithium storage properties *Electrochem. Commun.* **20** 7–10
[29] Silbernagel B G 1975 Lithium intercalation complexes of layered transition metal dichalcogenides: an NMR survey of physical properties *Solid State Commun.* **17** 361–5
[30] Whittingham M S 1978 Chemistry of intercalation compounds: metal guests in chalcogenide hosts *Prog. Solid State Chem.* **12** 41–99
[31] Friend R H and Yoffe A D 1987 Electronic properties of intercalation complexes of the transition metal dichalcogenides *Adv. Phys.* **36** 1–94
[32] Park J, Kim J S, Park J W, Nam T H, Kim K W, Ahn J H, Wang G X and Ahn H J 2013 Discharge mechanism of MoS_2 for sodium ion battery: electrochemical measurements and characterization *Electrochim. Acta* **92** 427–32
[33] Wang L F, Xu Z, Wang W L and Bai X D 2014 Atomic mechanism of dynamic electrochemical lithiation processes of MoS_2 nanosheets *J. Am. Chem. Soc.* **136** 6693–7
[34] Wang X F, Shen X, Wang Z X, Yu R C and Chen L Q 2014 Atomic-scale clarification of structural transition of MoS_2 upon sodium intercalation *ACS Nano* **8** 11394–400
[35] Santhosha A L, Nayak P K, Pollok K, Langenhorst F and Adelhelm P 2019 Exfoliated MoS_2 as electrode for all-solid-state rechargeable lithium-ion batteries *J. Phys. Chem.* C **123** 12126–34
[36] Winchester A, Ghosh S, Feng S M, Elias A L, Mallouk T, Terrones M and Talapatra S 2014 Electrochemical characterization of liquid phase exfoliated two-dimensional layers of molybdenum disulfide *ACS Appl. Mater. Interfaces* **6** 2125–30
[37] Bang G S, Nam K W, Kim J Y, Shin J, Choi J W and Choi S Y 2014 Effective liquid-phase exfoliation and sodium ion battery application of MoS_2 nanosheets *ACS Appl. Mater. Interfaces* **6** 7084–9
[38] Coleman J N *et al* 2011 Two-dimensional nanosheets produced by liquid exfoliation of layered materials *Science* **331** 568–71
[39] Wang X L *et al* 2014 Chemical vapor deposition growth of crystalline monolayer $MoSe_2$ *ACS Nano* **8** 5125–31
[40] Lu X *et al* 2014 Large-area synthesis of monolayer and few-layer $MoSe_2$ films on SiO_2 substrates *Nano Lett.* **14** 2419–25
[41] Late D J, Liu B, Ramakrishna Matte H S S, Rao C N R and Dravid V P 2012 Rapid characterization of ultrathin layers of chalcogenides on SiO_2/Si substrates *Adv. Funct. Mater.* **22** 1894–905
[42] Kim Y, Bark H, Ryu G H, Lee Z and Lee C 2016 Wafer-scale monolayer MoS_2 grown by chemical vapor deposition using a reaction of MoO_3 and H_2S *J. Phys.: Condens. Matter* **28** 184002
[43] Wang L *et al* 2019 Electronic devices and circuits based on wafer-scale polycrystalline monolayer MoS_2 by chemical vapor deposition *Adv. Electron. Mater.* **5** 1900393
[44] Peng L L, Zhu Y, Chen D H, Ruoff R S and Yu G H 2016 Two-dimensional materials for beyond-lithium-ion batteries *Adv. Energy Mater.* **6** 1600025
[45] Liu J H and Liu X W 2012 Two-dimensional nanoarchitectures for lithium storage *Adv. Mater.* **24** 4097–111
[46] Yang E, Ji H and Jung Y 2015 Two-dimensional transition metal dichalcogenide monolayers as promising sodium ion battery anodes *J. Phys. Chem.* C **119** 26374–80
[47] Schmidt P A, Schmitz P and Zaeh M F 2016 Laser beam welding of electrical contacts for the application in stationary energy storage devices *J. Laser Appl.* **28** 022423
[48] Geohegan D B *et al* 2018 Laser synthesis, processing, and spectroscopy of atomically-thin two dimensional materials *Advances in the Application of Lasers in Materials Science* ed P M Ossi (Cham: Springer) pp 1–37
[49] Mahjouri-Samani M *et al* 2015 Patterned arrays of lateral heterojunctions within monolayer two-dimensional semiconductors *Nat. Commun.* **6** 7749
[50] Ahmadi Z, Fathi-Hafshejani P, Kayali E, Beidaghi M and Mahjouri-Samani M 2021 Rapid laser nanomanufacturing and direct patterning of 2D materials on flexible substrates—2DFlex *Nanotechnology* **32** 055302
[51] Fathi-Hafshejani P, Johnson H, Ahmadi Z, Roach M, Shamsaei N and Mahjouri-Samani M 2021 Laser-assisted selective and localized surface transformation of titanium to anatase, rutile, and mixed phase nanostructures *J. Laser Appl.* **33** 012014
[52] Fathi-Hafshejani P, Johnson H, Ahmadi Z, Roach M, Shamsaei N and Mahjouri-Samani M 2020 Phase-selective and localized TiO_2 coating on additive and wrought titanium by a direct laser surface modification approach *ACS Omega* **5** 16744–51
[53] Ahmadi Z, Fathi-Hafshejani P and Mahjouri-Samani M 2021 Laser patterning and crystallization of 2D materials on rigid and flexible substrates *Proc. SPIE* **11675** 116750C
[54] Liu H Z, Zhang G H, Zheng X, Chen F J and Duan H G 2020 Emerging miniaturized energy storage devices for microsystem applications: from design to integration *Int. J. Extrem. Manuf.* **2** 042001
[55] Fathi-Hafshejani P, Soltani-Tehrani A, Shamsaei N and Mahjouri-Samani M 2022 Laser incidence angle influence on energy density variations, surface roughness, and porosity of additively manufactured parts *Addit. Manuf.* **50** 102572
[56] Pfleging W 2018 A review of laser electrode processing for development and manufacturing of lithium-ion batteries *Nanophotonics* **7** 549–73
[57] Habedank J B, Endres J, Schmitz P, Zaeh M F and Huber H P 2018 Femtosecond laser structuring of graphite anodes for improved lithium-ion batteries: ablation characteristics and process design *J. Laser Appl.* **30** 032205
[58] Tsuda T *et al* 2018 Improvement of high-rate charging/discharging performance of a lithium ion battery

composed of laminated $LiFePO_4$ cathodes/ graphite anodes having porous electrode structures fabricated with a pico-second pulsed laser *Electrochim. Acta* **291** 267–77
[59] Park J, Hyeon S, Jeong S and Kim H J 2019 Performance enhancement of Li-ion battery by laser structuring of thick electrode with low porosity *J. Ind. Eng. Chem.* **70** 178–85
[60] Pfleging W 2021 Recent progress in laser texturing of battery materials: a review of tuning electrochemical performances, related material development, and prospects for large-scale manufacturing *Int. J. Extrem. Manuf.* **3** 012002
[61] Tang X X, Liu W, Ye B Y and Tang Y 2013 Preparation of current collector with blind holes and enhanced cycle performance of silicon-based anode *Trans. Nonferr. Met. Soc. China* **23** 1723–7
[62] Zheng Y, An Z, Smyrek P, Seifert H J, Kunze T, Lang V, Lasagni A F and Pfleging W 2016 Direct laser interference patterning and ultrafast laser-induced micro/nano structuring of current collectors for lithium-ion batteries *Proc. SPIE* **9736** 97361B
[63] Notten P H L *et al* 2007 3D integrated all-solid-state rechargeable batteries *Adv. Mater.* **19** 4564–7
[64] Ferrari S, Loveridge M, Beattie S D, Jahn M, Dashwood R J and Bhagat R 2015 Latest advances in the manufacturing of 3D rechargeable lithium microbatteries *J. Power Sources* **286** 25–46
[65] Zhang H G, Yu X D and Braun P V 2011 Three-dimensional bicontinuous ultrafast-charge and -discharge bulk battery electrodes *Nat. Nanotechnol.* **6** 277–81
[66] Pröll J, Kim H, Piqué A, Seifert H J and Pfleging W 2014 Laser-printing and femtosecond-laser structuring of $LiMn_2O_4$ composite cathodes for Li-ion microbatteries *J. Power Sources* **255** 116–24
[67] Kim J S, Pfleging W, Kohler R, Seifert H J, Kim T Y, Byun D, Jung H G, Choi W and Lee J K 2015 Three-dimensional silicon/carbon core–shell electrode as an anode material for lithium-ion batteries *J. Power Sources* **279** 13–20
[68] Rau H, Kutty T R N and De Carvalho J R F G 1973 Thermodynamics of sulphur vapour *J. Chem. Thermodyn.* **5** 833–44
[69] Park S J, Chung Y D, Lee W J, Cho D H, Wi J H, Han W S, Cho Y and Yoon J M 2015 Flexible solar cells with a Cu (In, Ga) Se_2 absorber grown by using a Se thermal cracker on a polyimide substrate *J. Korean Phys. Soc.* **66** 76–81
[70] Li H, Zhang Q, Yap C C R, Tay B K, Edwin T H T, Olivier A and Baillargeat D 2012 From bulk to monolayer MoS_2: evolution of Raman scattering *Adv. Funct. Mater.* **22** 1385–90
[71] Carvalho B R, Wang Y X, Mignuzzi S, Roy D, Terrones M, Fantini C, Crespi V H, Malard L M and Pimenta M A 2017 Intervalley scattering by acoustic phonons in two-dimensional MoS_2 revealed by double-resonance Raman spectroscopy *Nat. Commun.* **8** 14670
[72] Bozheyev F, Valiev D and Nemkayeva R 2017 Pulsed cathodoluminescence and Raman spectra of MoS_2 nanocrystals at different excitation electron energy densities and laser wavelengths *J. Lumin.* **188** 529–32
[73] Miki Y, Nakazato D, Ikuta H, Uchida T and Wakihara M 1995 Amorphous MoS_2 as the cathode of lithium secondary batteries *J. Power Sources* **54** 508–10
[74] Ding S J, Chen J S and Lou X W 2011 Glucose-assisted growth of MoS_2 nanosheets on CNT backbone for improved lithium storage properties *Chem. Eur. J.* **17** 13142–5
[75] Wang P P, Sun H Y, Ji Y J, Li W H and Wang X 2014 Three-dimensional assembly of single-layered MoS_2 *Adv. Mater.* **26** 964–9
[76] Ding S J, Zhang D Y, Chen J S and Lou X W 2012 Facile synthesis of hierarchical MoS_2 microspheres composed of few-layered nanosheets and their lithium storage properties *Nanoscale* **4** 95–98
[77] Zhang C F, Wang Z Y, Guo Z P and Lou X W 2012 Synthesis of MoS_2–C one-dimensional nanostructures with improved lithium storage properties *ACS Appl. Mater. Interfaces* **4** 3765–8
[78] Pfleging W and Gotcu P 2019 Femtosecond laser processing of thick film cathodes and its impact on lithium-ion diffusion kinetics *Appl. Sci.* **9** 3588